A numerical reconstruction of fall deposits from the Agnano-Monte Spina (4100 BP) Plinian eruption in the Campi Flegrei area, Italy

Pfeiffer, T.[1,2], Costa, A.[2]

[1] Department of Earth Sciences, University of Aarhus, Denmark

[2]Osservatorio Vesuviano, Naples, Italy

Osservatorio Vesuviano – INGV
Via Diocleziano, 328
I-80124 Naples, Italy

Technical Report (1)
on the Scientific Collaboration OV-INGV Contracts Number:
909 (15-05-01)
1129 (26-06-03)
1134 (30-09-03)

Research Unit Responsible: Giovanni Macedonio

A numerical reconstruction of fall deposits from the Agnano-Monte Spina (4100 BP) Plinian eruption in the Campi Flegrei area, Italy

Pfeiffer, T.[1,2], Costa, A.[2]

Abstract

A simple semianalytical model was applied to simulate the tephra deposits produced by two Plinian phases called B1 and D1 of the Agnano-Monte Spina eruption (4100 BP) within the Campli Flegrei volcanic area in Italy. In this model, the eruption column is assumed to act as a line source in order to neglect complex near/vent interactions. Therefore, the validity of the model is limited to the medium and far areas from the vent (beyond 10-20km), where the assumption of a line source can be justified. The distribution of the particles in the atmosphere is assumed to be only controlled by gravity, wind and eddy diffusion. The model accounts for particles of different types and (juvenile pumice or ash particles, lithic fragments and crystals) within an used-defined range of granulometric classes.
The numerically calculated deposit was confronted with the observed deposit. Applying a least/squares method it was tried to optimize input variables such as distribution of particles and mass within the eruption column, wind and diffusion parameters by fitting the computed deposit with the observed one. A good correlation between the numerically calculated and the measured deposit as well as a good agreement between the fitted variables with independently found parameters of the eruption could be achieved. The results allowed to re-estimate eruption parameters such as minimum erupted mass (2-3x10^{11} kg each), eruption column height (16-23 km for B1, ca. 30 km for D1), grain-size spectrum of erupted tephra, and the wind field at the time of the eruption.

1. Introduction: the AMS eruption

The A.M.S. (Agnano-Monte Spina) eruption at ca. 4100 BP was the largest explosive event during the last activity cycle of the Campi Flegrei volcanic field. The eruption probably took place in the Agnano plain near Naples and has been described in detail by De Vita et al. (1999). Its deposits include alternating layers of fall and flow deposits. Two wide-spread prominent pumice fall-out layers, labeled B1 and D1 in De Vita et al. (1999) have been interpreted as fall-out from Plinian convecting eruption columns. In this study, a previously developed and recently modified numerical model is applied to reconstruct these fall deposits and constrain eruption parameters such as erupted mass, component and grain-size spectrum of erupted mass, eruption column height and wind at the time of the eruption.
The numerical reconstruction was performed using an well-established 2-dimensional diffusion-advection-sedimentation model that is described in detail in Pfeiffer et al. (2004) and Pfeiffer (2003). However, a brief outline of the physical principles and its solution is presented in the following paragraphs.
[2]

2. The physical model

Far from the vent, the internal dynamic effects of eruption columns are neglected in order to describe the dispersion and sedimentation of tephra. Under this assumption, the motion of particles can be described sufficiently by wind transport, turbulent diffusion and settling of particles by gravity. As a consequence, the model is only valid sufficiently far from the vent, at a distance comparable to the eruption column height (e.g. Armienti et al., 1988) and its results are therefore only relevant in the medium-distal area, where tephra fall commonly is the major volcanic hazard.
The mass conservation equation for each class of particles with given settling velocity may be generally written as:

[1] Department of Earth Sciences, University of Aarhus, Denmark, Email: tpfeiffer@decadevolcano.net
[2] Osservatorio Vesuviano, V. Diocleziano, 328, Naples, Italy, Email: costa@ov.ingv.it

$$\frac{\partial C}{\partial t}+\frac{\partial (w_x C)}{\partial x}+\frac{\partial (w_y C)}{\partial y}+\frac{\partial (w_z C)}{\partial z}-\frac{\partial (v_{settl} C)}{\partial z}=K_x\frac{\partial^2 C}{\partial x^2}+K_y\frac{\partial^2 C}{\partial y^2}+K_z\frac{\partial^2 C}{\partial z^2}+S \qquad (1)$$

where C is the concentration of particles, t time, x, y, z spatial coordinates, w_i the wind field, K_i the eddy diffusion coefficients ($i = x, y, z$), $v_{settl}:=v_s$ settling velocity and S a source function describing the influx of mass from the eruption column. Eq. (1) is valid for each class j of particles having a given settling velocity v_s.

2.1. Eruption column and vertical mass distribution

In this model, the eruption column acts as a vertical line source. Since this simplification is only valid far from the vent, the use of the model is limited to areas sufficiently far from the vent. The results from Macedonio et al. (1988) and Armienti et al. (1988) suggest that this critical distance is approximately given by the height of the eruption column itself. Since eq. (1) is linear in mass, an instantaneous release of the total mass from the eruption column can be assumed if wind and diffusion parameters do not change significantly with time. Variations of the eruption column with time are in this approach replaced by a time-averaged column.
To describe the vertical mass distribution in an eruption column, a modified version of the formula suggested by Suzuki (1983) is applied. It describes the vertical mass concentration uniformly for all particle classes as:

$$S(x,y,z,t)=S_0\left\{\left(1-\frac{z}{H}\right)\exp\left[A\left(\frac{z}{H}-1\right)\right]\right\}\delta(t-t_0)\delta(x-x_0)\delta(y-y_0) \qquad (2a)$$

where S(z):={1-z/H exp [A/(z/H-1]} is the vertical mass distribution function, z the altitude in the eruption column, S_0 a normalization factor, H the maximum plume height, A a dimensionless parameter ("Suzuki coefficient") and δ is the Dirac's distribution (punctual and instantaneous release assumption). Eq. (2a) is considered a merely empirical description of the vertical mass distribution within the eruption column with a purely geometric meaning. The value of A describes the vertical position of the maximum concentration relative to the maximum column height, located at (A-1)/A of the maximum plume height (Fig. 1a).
Theoretical and empirical observations on buoyant plumes (e.g. Morton et al., 1956; Sparks, 1986) show that the ratio H_B/H_T between the height of buoyancy of the plume H_B and its maximum height H_T is usually around 3/4. This is here accounted for by setting A=4 in eq. (2a). Instead of using A, a different parameter called λ is introduced:

$$S(z)=S_0\left\{\left(1-\frac{z}{H}\right)\exp\left[A\left(\frac{z}{H}-1\right)\right]\right\}^{\lambda} \qquad (2b)$$

The value of the parameter λ is a measure of how strongly the total mass is concentrated around the maximum concentration at H(A-1)/A (Fig. 1b). Only the second factor λ was varied between values of 1, 1.5,…, 5.

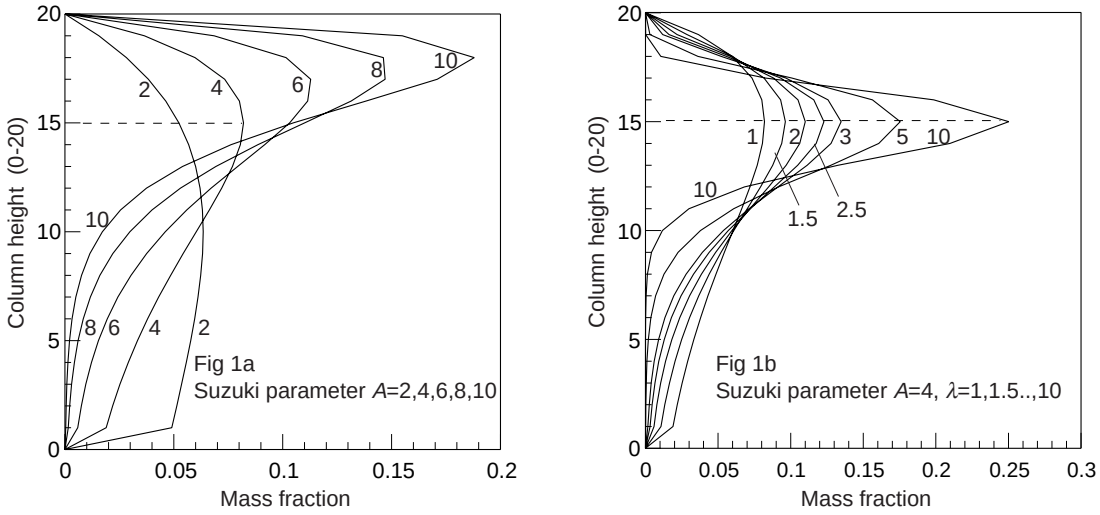

Fig. 1. Models describing the vertical mass distribution (here for a 20 km high eruption column) according to the modified formula of Suzuki (1983) (eq. 2a/b). The values of the Suzuki parameters A and l were varied between A=2, 4, 6, 8, 10 with λ =1 (Fig. 1a) and λ=1, 1.5, 2, 2.5, 3, 5, 10 with A=4 (Fig. 1b).

2.2. Atmospheric turbulent diffusion, wind translation and deposition

Following previous studies (e.g. Armienti et al., 1988), both vertical diffusion and wind components are usually of an order of magnitude smaller than the horizontal components and are therefore neglected in this model. In addition it is assumed:

(1) Eddy diffusion acts homogeneously in all horizontal directions, and thus $K_x=K_y := K$.

(2) The diffusion coefficient $K_{x,y}$ is constant. Horizontal wind components vary only with altitude z.

(3) Horizontal wind components are constant in time and within the horizontal domain. This assumption should hold for intermediate distances of the order of 50-100 km or more, but becomes increasingly wrong with large distances.

Under these additional assumptions, eq. (1) simplifies to:

$$\frac{\partial C}{\partial t}+\frac{\partial (w_x C)}{\partial x}+\frac{\partial (w_y C)}{\partial y}-\frac{\partial (v_{sett} C)}{\partial z}=K\frac{\partial^2 C}{\partial x^2}+K\frac{\partial^2 C}{\partial y^2}+S \qquad (3)$$

Eq. (3) is solved by using the semi-analytical method described in Pfeiffer et al. (2004) and Macedonio et al. (2004). This model assumes that each class of particles (with the same settling velocity) has a Gaussian-shaped distribution in each horizontal layer at any time:

$$C(x,y,z,t)=\frac{C_0^*}{4\pi Kt}\exp\left[-\frac{(x-x_c)^2+(y-y_c)^2}{4Kt}\right] \qquad (4)$$

where C_0* is a normalization factor and $x_c=w_x t$, $y_c=w_y t$ the center coordinates of the Gaussian wind-advected cloud. Therefore, the 4-dimensional domain is split into thin horizontal layers that 'fall' to the ground together with the particles originally contained in a given initial vertical interval [z1; z2] at time t=0. A solution in the form of eq. (4) is then found for each layer. Since the whole treatment is done separately for each class of particles and no vertical diffusion and wind advection takes place, all particles falling from the same initial height remain at all times at the same altitude. While the center of each cloud is translated by wind, the cloud spreads horizontally due to diffusion and settles by gravity until it reaches the ground where it forms the deposit. For more details of the mathematical description of the model see Pfeiffer et al. (2004) and Macedonio et al. (2004).

2.3. Settling velocity of particles

Settling velocity of volcanic particles is a complex function of particle size, shape and density and depends also on density and viscosity of the surrounding air. Its value can only be computed approximately and relies heavily on empirical data. In this study, it is calculated for each size and component class at each altitude separately, according to Pfeiffer et al. (2004) and Pfeiffer (2003) who presented a set of formula that represents a best fit to available experimental data on pyroclastic particles.
Since particle settling velocity changes with altitude and Reynolds number, only particles with the same size, shape and density can be strictly regarded as belonging to a given settling velocity class (for details see Pfeiffer et al., 2004). Particles with different densities that belong to a given settling velocity class at a given altitude can have different settling velocities at other altitudes, depending on their different Reynolds numbers. It is therefore better and more correct to treat each size class of each present component as a single settling velocity class, rather than simply dividing the bulk settling velocity spectrum (containing all components) at a given altitude, e.g. at sea level, into pure settling classes of (mixed component) particles, which has been a commonly used method in the past (e.g. Armienti et al., 1988).

3. Numerical modeling of the AMS eruption and input parameters

The numerical model outlined in the previous chapter was performed using a FORTRAN code called "ashfall" (Version 57 as of 19 Oct. 2003, by T. Pfeiffer, unpublished), based on the program "Hazmap" by Macedonio et al. (2004). The program requires a number of input parameters, which either can be assigned fixed values or can be treated as free variables that are fitted to best match an observed deposit according to user-defined criteria. These parameters, together with the best-fitting results, are summarized in Tab. 2:

- Maximum height of the eruption column H. This parameter was allowed to vary between 10 and 35 km.
- Number and spacing of vertical source points to model the eruption column. In this study, 40 equally spaced source points were taken.
- Vertical mass distribution in the eruption column. The factor `l` in eq. (2) was varied between 1 and 5.
- Constant eddy diffusion coefficient K. This parameter was varied between 2000 and 7000 m^2/s.
- Total mass. It was found by best fitting the calculated with the measured deposit.
- Wind speed and direction at given levels. See respective chapter 3.2.
- Initial bulk component, particle density and grain-size spectrum of erupted tephra. See respective chapter 3.3.
- Average void fraction of deposit. This was here assumed as 25 vol% and the resulting void volume was added to the calculated fully compacted deposit, which was computed as the sum of all (density-dependent) volume contributions of each particle class depositing in each point on the ground. The program thus calculates mass accumulation per area and thickness (or deposit density) simultaneously.

3.1 Field data and fitting method

Fitting was performed using a least-square method comparing measured and calculated data. Because of the inherent limitation of the model to medium-range and far parts of a deposit, only available data from samples at at least 10 km distance from the center of the Agnano plain (the assumed vent area) were considered. The data used here were either taken directly from De Vita et al. (1999) and Tesauro (2000) or represent still unpublished field data (kindly made available by researchers at the Osservatorio Vesuviano, Naples, belonging to the team around Orsi).
To compensate for the nevertheless relatively close range of some sample points considering that the estimated eruption column heights might between 15 and 30 km, weighting of samples against each other as a function of distance was introduced: Between 10 and 20 km, progressively increasing weight from 0 to 1

was given, and weight 1 for all samples at distances greater than 20 km. Afterwards, all weights were renormalized.
Since fitting parameters of different nature are involved (total deposit thickness and mass fraction of distinct component-grain-size classes data), the correct assessment of errors is important. In detail, the following relative and absolute minimum errors were used:

- Error in measurement of the total deposit thickness: 20% relative error, at least 1cm.
- Error in deposit density: 30% relative error, at least 1 wt%.

Additionally, in order to account for the smaller number of fitting data for the total deposit values (30 and 25 data for B1 and D1) against the number of usable grain-size data (9 classes x 3 components x 4/5 sample locations = 108/135 fitting data), the total least square error of the total deposit was weighted 1.6 and the total least square error of the grain-size data by 0.4.

3.2. Bulk component and grain-size spectrum of erupted tephra

The initial bulk component and grain-size composition of erupted tephra is a crucial requirement for the model. Three independent components were used, pumice, lithics and crystals. For the model, only the densities of the components matter. For lithics and crystals, grain-size independent constant densities of 2,500 and 2,700 kg/m^3 were applied, whereas the density of pumice was taken as grain-size dependant using typical values similar to those measured at pumice from Vesuvius (79 A.D. eruption, gray pumice, reported in Macedonio et al., 1988). These values are given in Tab. 1.

Tab. 1. Grain-size dependant density of juvenile pumice as used in the model. Data modified after Macedonio et al (1988), who report density data of juvenile pumice from Vesuvius 79 A.D. Gray Pumice deposit.

Φ	**Density**
<= -1.5	650 kg/m^3
-0.5	900 kg/m^3
0.5	1150 kg/m^3
1.5	1430 kg/m^3
2.5	1720 kg/m^3
3.5	2010 kg/m^3
>= 4	2300 kg/m^3

Unfortunately, the original grain-size distribution of each component cannot be obtained by direct observation unless large parts of the deposit are preserved and analyzed, which is not the case. For B1, only 4 samples with known component and grain-size spectrum, and for D1 only 5 such data sets are available. Therefore, Rosin's law of Gaussian-distributed logarithmic grain-size was applied. For each component, the mean grain size $\mu(\Phi)$ and the standard deviation $\sigma(\Phi)$ were free parameters found by best fitting and the total mass of each component was then accordingly distributed into the interval $[-6<\Phi<+6]$. The resulting spectra are given in Fig. 2.

3.3.Wind

Vertical wind components are neglected in the model because they are on an average of an order of magnitude smaller than horizontal components. Three different wind models (W1, W2 and W3) were applied to the reconstruction of the AMS fall-out tephra. The used wind profiles are given in Fig. 3.
In the first model W1, wind speeds from a measured wind profile for southern Italy (summer wind profile from Cornell et al., 1983) are scaled with a factor found by best fitting, whereas all wind vectors have the same direction, which is found by best fitting.
In the second wind model (W2), a generic wind profile is found by best fitting. It assumes linearly increasing wind speeds from 4 m/s on the ground to a variable, best-fitted wind maximum wind speed at the tropopause level, here taken at 10.8 km altitude, and a second best fitted constant wind speed above 15 km altitude. Wind speeds at intermediate levels between 10.8 and 15 km are linearly interpolated. As in W1, all wind directions point in the same direction.
W3 is similar to W2, but also allows a different wind direction for all wind vectors above 15 km, while wind directions between 10.8 and 15 km are also interpolated. Although the model concept of diffusion takes account for the proximal effect of moderate normal wind shear between different levels (compare Pfeiffer,

2003), a significant effect remains if wind directions within lower and higher atmospheric levels are very much different. In southern Italy, this is typically the case during the summer season, as the corresponding wind profile from Cornell et al. (1983) shows (Fig. 3). In contrast, winds are blowing rather consistently from westerly directions at all levels during the rest of the year (Cornell et al., 1983). As an example, the autumn wind profile is shown in Fig. 3. Thus, the application of W2, where different wind directions below and above the tropopause are allowed, serves as a test to judge whether the eruption might have taken place during summer or not.

4. Results and Discussion

For all runs (using the 3 different wind models) the numerically calculated deposits of B1 and D1 were in good agreement with the measured ones, including a good agreement for the grain-size spectra in the 4 (B1) or 5 (D1) available sample points. The results are summarized in Tab. 2-4 and Figs. 2-13.
When fitting the model for D1, the diffusion coefficient takes the highest allowed value of 7,000 m/s^2; if left to vary freely, the best fitting values would be unrealistically high, around 30,000 m/s^2. This probably reflects in the first place the inferior field data quality in the case of D1, where the lateral limits of the deposit are not well-defined. Another argument is that the assumption of a relatively uniform wind field is less correct than for the narrower and much better defined deposit B1.
For both deposits, modeling improves slightly, if the wind profile is decoupled from the summer wind profile and a hypothetic wind profile is established using best-fitting parameters. In particular, the runs using wind models W2 and W3 allow higher wind speeds at great altitude. The difference between W2 and W3 is finally the fact that W3 also allows a different wind direction at great altitude (above 15 km). For both deposits, high southwesterly and similar wind directions provide the best fit, which is a suggestion that the assumption is realistic. The resulting wind profiles of runs 2 and 3 for B1 and D1 (Fig. 2) are then not too different from the typical autumn wind profile. This suggests that the eruption might not have taken place in summer, where high altitude winds are likely to blow from the E.

Maximum eruption column heights were difficult to asses because this parameter is strongly correlated with the parameters describing vertical mass distribution. While the variation of the latter was only varied in a relatively narrow range, fixing the first parameter in eq. (2a) A=4 and varying the second one l between 1 and 5, best fitting eruption column heights still varied between 16 and 23 km for B1, and 30 and 35 km for D1, according to which wind model was used. It is also noted, that variations of the column height of the order of a few km did not significantly change the resulting fit. In runs B1-2 and D1-2, the eruption column heights were fixed at 20 and 30 km. The estimate provided by this model can therefore only be seen as a rough approximation correct probably only to the order of around 5-10 km.
On the other hand, the values obtained here are in good agreement with De Vita et al.' s (1999) own estimates who used the method of Carey and Sparks (1986), obtaining 23 and 27 km maximum heights for B1 and D1 respectively, although some doubt about the accuracy of their original estimates have arisen (de Vita et al., pers. com.).
The mass estimates provided here vary not significantly between different runs. According to our results, both deposits account for around 2.5×10^{11} kg each, or 10^8 m^3 DRE (using a rock density 2500 kg/m^3). As shown in previous studies (e.g. Pfeiffer et al., 2004), the estimates are reliable as estimates of the mass contained in the study area only. The true erupted mass might be significantly higher, since the very fine fraction is not accounted for because of the lack of distal data. The total mass of the AMS B1 and D1 tephra deposits might therefore be corrected by a factor, which is difficult to assess, but is thought to be in the range of 30-50%.
Concerning the limitation of the model in the close range, the model does not include the large clasts falling in these proximal areas. However, the mass deposited in the very proximal area (less than 10 km) of fall deposits is very small to the total mass of the deposit and does not significantly affect the mass estimate by the model, which could easily be shown by calculating the mass within this area and comparing it to the model mass (e.g. Pfeiffer, 2003).

5. Conclusion

Despite the simplicity of the model and the assumptions involved, the results of the modeling of the A.M.S. eruption support its validity. It has the advantage to be extremely simple and fast to compute. It provides a both practical and physical plausible use from areas from ca. 10 km away from the source of an eruption. This is the zone outside of the area of active volcanoes where other volcanic hazards, mainly pyroclastic flows constitute the major hazard. Therefore, it has the potential to serve as a simple tool to predict the ash fall for hypothetical eruptions of a given magnitude and a given wind profile and can readily be applied to the case of the volcanoes of the area around the Naples bay. It could not only be used to reconstruct past eruptions, but also to construct tephra-fall hazard maps of the most likely affect areas around active volcanoes where a larger eruption is expected to occur. The quality of such prediction is strongly dependent on as much information about typical eruption parameters as grain-size distribution, settling velocity of particles and local wind fields as possible. Future work should be aimed at providing such data.

Acknoledgements

Component analysis performed by Tesauro (2000) were used in this study. M. Di Vito is acknowledged for providing part of field data. Tom Pfeiffer was partially supported by the EU community programme "Research Training Network in Volcanology" (2002).

Tab. 2. Input parameters and best-fitting values.

	B1			D1		
Run	**B1-1 (W.model 1)**	**B1-2 (W. model 2)**	**B1-3 (W.model 3)**	**D1-1 (W.model 1)**	**D1-2 (W.model 2)**	**D1-3 (W.model 3)**
Parameter						
Number of Φ-classes	24	24	24	24	24	24
Number of source points	40	40	40	40	40	40
Total mass	$2.3x10^{11}$ kg	$2.8x10^{11}$ kg	$2.7x10^{11}$ kg	$2.8x10^{11}$ kg	$2.5x10^{11}$ kg	$2.5x10^{11}$ kg
Column height	16 km	20 km (fix)	23 km	35 km	30 km (fix)	30 km
Suzuki constant λ, (A=4 fix)	3	2	2	1	1	1
Pumice						
Gaussian mean μ(Φ)	-0.6	-0.1	-0.2	0.5	-0.6	-0.6
Standard deviation σ(Φ)	3.0	3.0	3.0	2.7	2.2	2.1
Wt %	40	40	40	40	40	40
Lithic fragments						
Gaussian mean μ(Φ)	1.2	1.4	1.5	0.5	0.1	0.3
Standard deviation σ(Φ)	1.4	1.6	1.6	1.4	1.3	1.4
Wt %	29	27	32	37	36	39
Crystals						
Gaussian mean μ(Φ)	2.3	3.4	2.5	2.0	2.5	2.1
Standard deviation σ(Φ)	1.3	2.0	1.5	1.2	1.7	1.4
Wt %	31	33	28	23	24	21
Diffusion coefficient	5,000 m^2/s	4,500 m^2/s	3,500 m^2/s	7,000 m^2/s	7,000 m^2/s	7,000 m^2/s
Wind direction <11 km	249° WSW	249° WSW	250° WSW	239° SW	240° SW	234° SW
Max. w. speed at 11 km	37 m/s	27 m/s	20 m/s	26 m/s	20 m/s	20 m/s
Wind direction >15km	249° WSW	249° WSW	242° SW	239° SW	240° SW	255° WSW
Wind speed >20 km	7-14 m/s	25 m/s	25 m/s	4-9 m/s	25 m/s	25 m/s
χ^2 (total deposit)	66.49	66.67	67.43	55.43	63.40	56.44
χ^2 (grain-size spectra)	238.5	257.9	223.1	259.6	192.83	182.0
Weighted $\chi^2 = 1.6\ \chi^2_{tot.} + 0.4\ \chi^2_{grainsize}$	201.8	209.67	196.4	192.5	178.6	163.1
Degrees of freedom n_F (number data – free variables)	(30+4*3*9) 138-14=124	(30+4*3*9) 138-14=124	(30+4*3*9) 138-16=122	(25+5*3*9) 160-14=146	(25+5*3*9) 160-14=146	(25+5*3*9) 160-15=144
Reduced $\chi^2_{red} = \chi^2 / n_F$	1.63	1.70	1.61	1.32	1.22	1.13

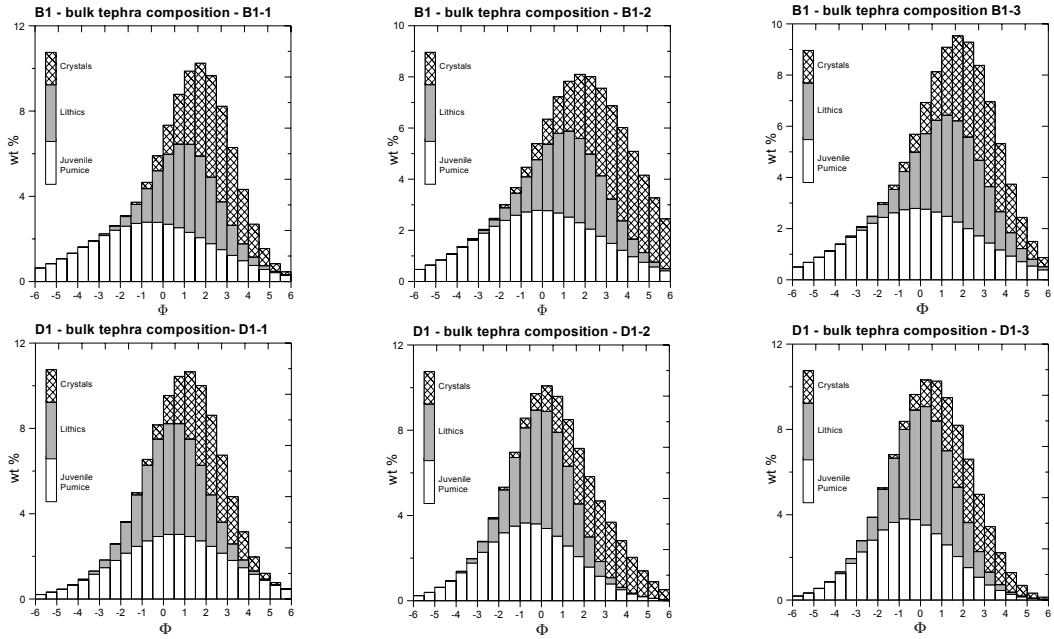

Fig. 2. Used bulk component grain-size distributions in model runs B/D1-1-3 (wind models 1-3) as obtained from best fitting.

References

Armienti, P., Macedonio, G., Pareschi, M.T. (1988). A Numerical Model for Simulation of Tephra Transport and Deposition: Application to May 18, 1980, Mount St. Helens Eruption - Journal of Geophysical Research 93, p.6463-6476.

Carey, S. and Sparks, R.S.J. (1986). Quantitative models of the fallout and dispersal of tephra from volcanic eruption columns. Bulletin of Volcanology, 48 (2/3), 127-141.

Cornell, W., Carey, S., Sigurdsson, H. (1983). Computer simulation and transport of the Campanian Y-5 ash, Journal of Volcanology and Geothermal Research, 17, 89-109.

De Vita, S., Orsi, G., Civetta, L., Carandente A., D'Antonio, M., Deino, A., di Cesare, T., Fisher, R.V., Isaia, R., Marotta, E., Necco, A., Ort, M.H., Pappalardo, L., Piochi, M., Southon, J. (1999). The Agnano-Monte Spina eruption (4100 years B.P.) in the restless Campi Flegrei caldera. Journal of Volcanology and Geothermal Research, 91, p. 269-301.

Macedonio, G., Pareschi, M.T., Santacroce, R. (1988). A Numerical Simulation of the Plinian Fall Phase of 79 A.D. Eruption of Vesuvius - Journal of Geophysical Research, 93, p. 817-827.

Macedonio, G., Costa A., Longo, A. (2004). Computer model of volcanic ash fall-out sustained columns and hazard assessment. Accepted for the pubblication on Computer & Geosciences.

Pfeiffer, T. (2003) Numeric reconstruction of tephra-fall deposits from the 18 august and 16/17 September 1992 eruptions of Crater Peak, Mt. Spurr volcano, Alaska, in: Two catastrophic volcanic eruptions in the Mediterranean – Santorini 1645 B.C. and Vesuvius 79 A.D., Ph.D. thesis, Dep. of Earth Sciences, University of Aarhus, Denmark, 141-183.

Pfeiffer, T., Costa A., Macedonio, G. (2004) A model for the numerical reconstruction of tephra-fall deposits, Journal of Volcanology and Geothermal Research, in press.

Suzuki, T. (1983) A theoretical model for dispersion of tephra. In: Volcanism: Physics and Tectonics, edited by D. Shimozuru and I. Yokoyama, pp. 95-113, Arc, Tokyo.

Tesauro, M. (2000) Relazione finale per la Borsa di studio annuale Alta Formazione - Progetto “Il Vulcanesimo dell’ area campana in relazione alla dinamica regionale, Osservatorio Vesuviano, Naples.

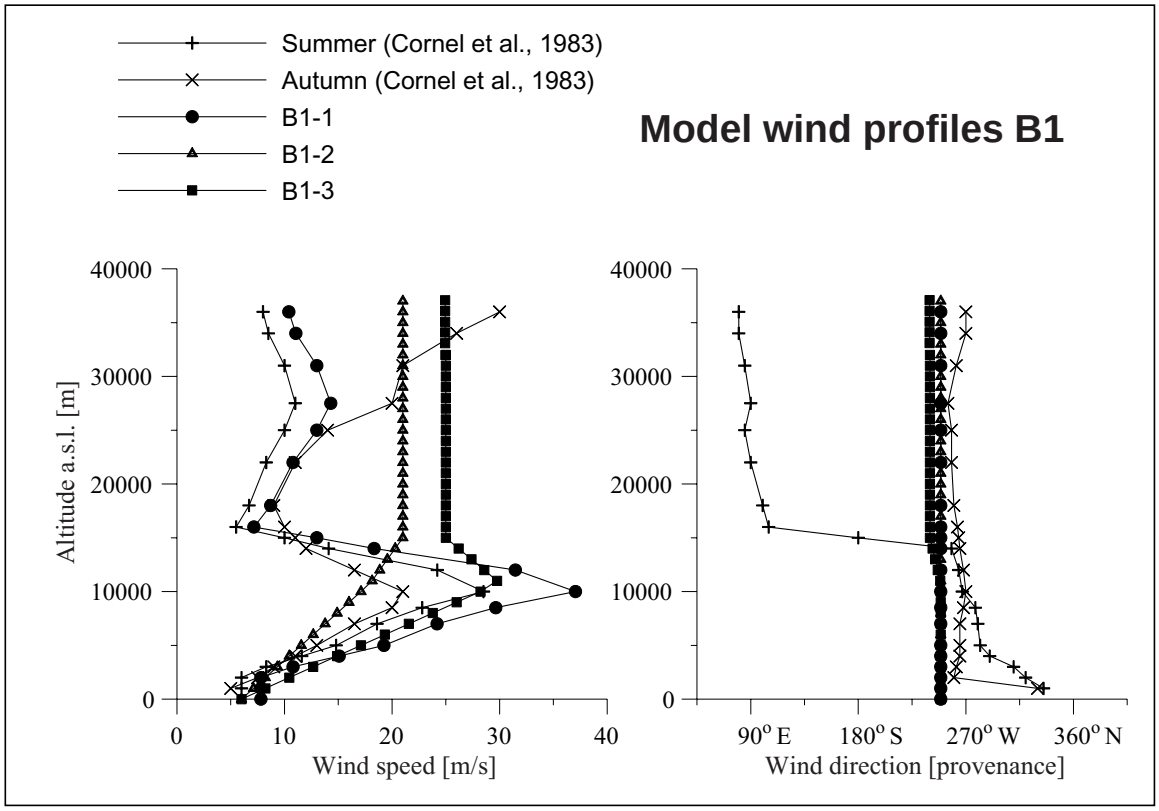

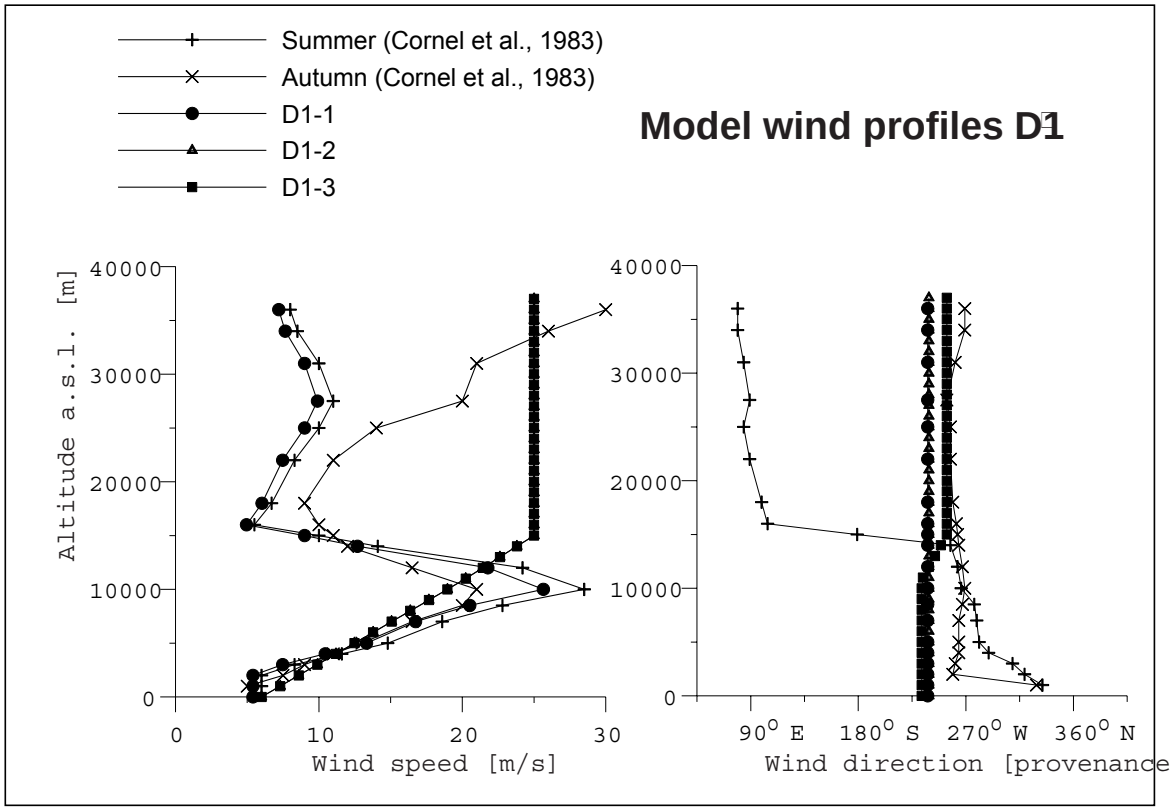

Fig. 3. Wind profiles used in the reconstructions and summer and autumn wind profiles for southern Italy from Cornell et al. (1983).

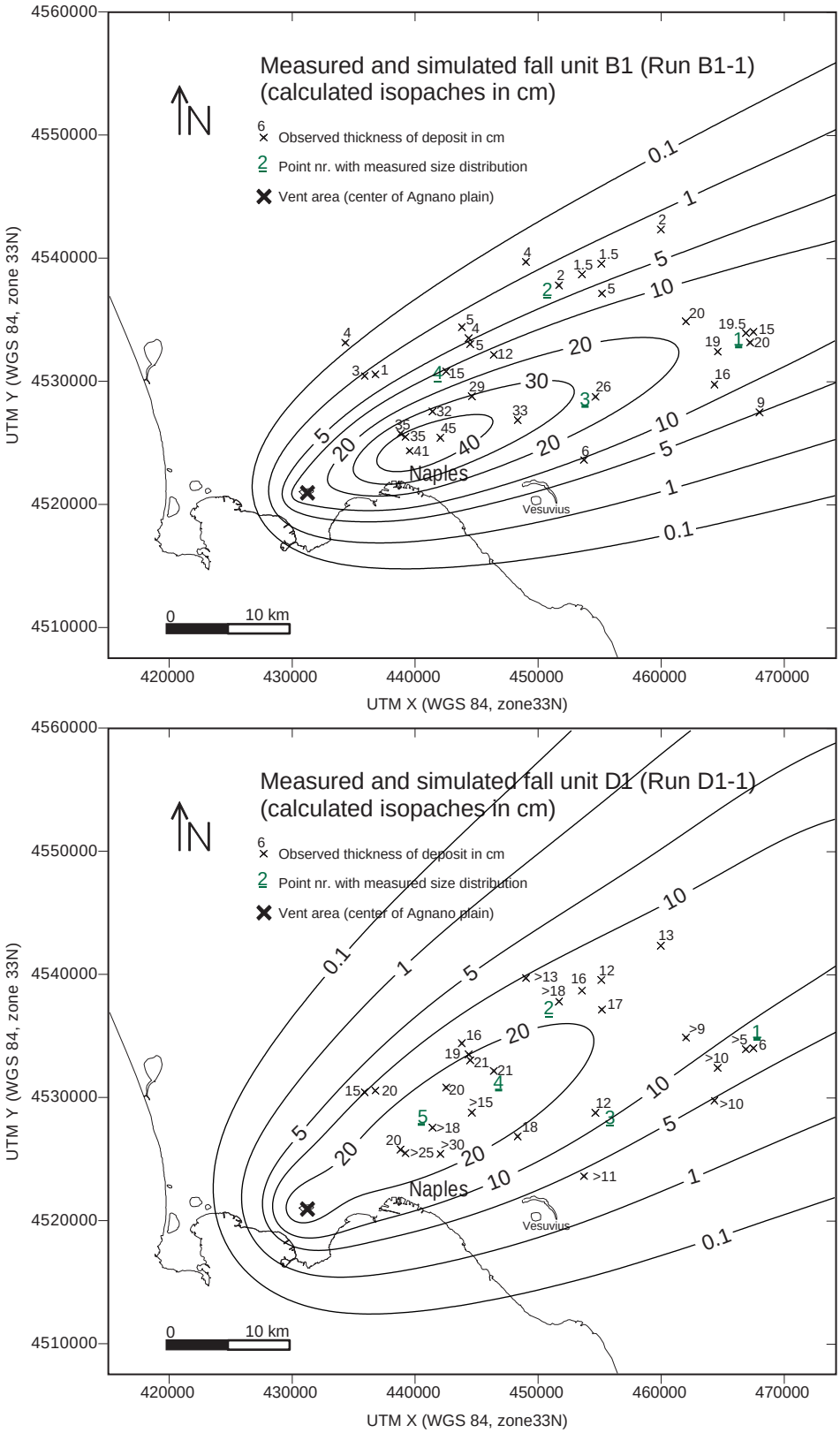

Fig. 4. Calculated isopachs and measured deposit thickness in cm of B1 and D1 fall deposits for Runs B1-1 and D1-1 (Wind model 1).

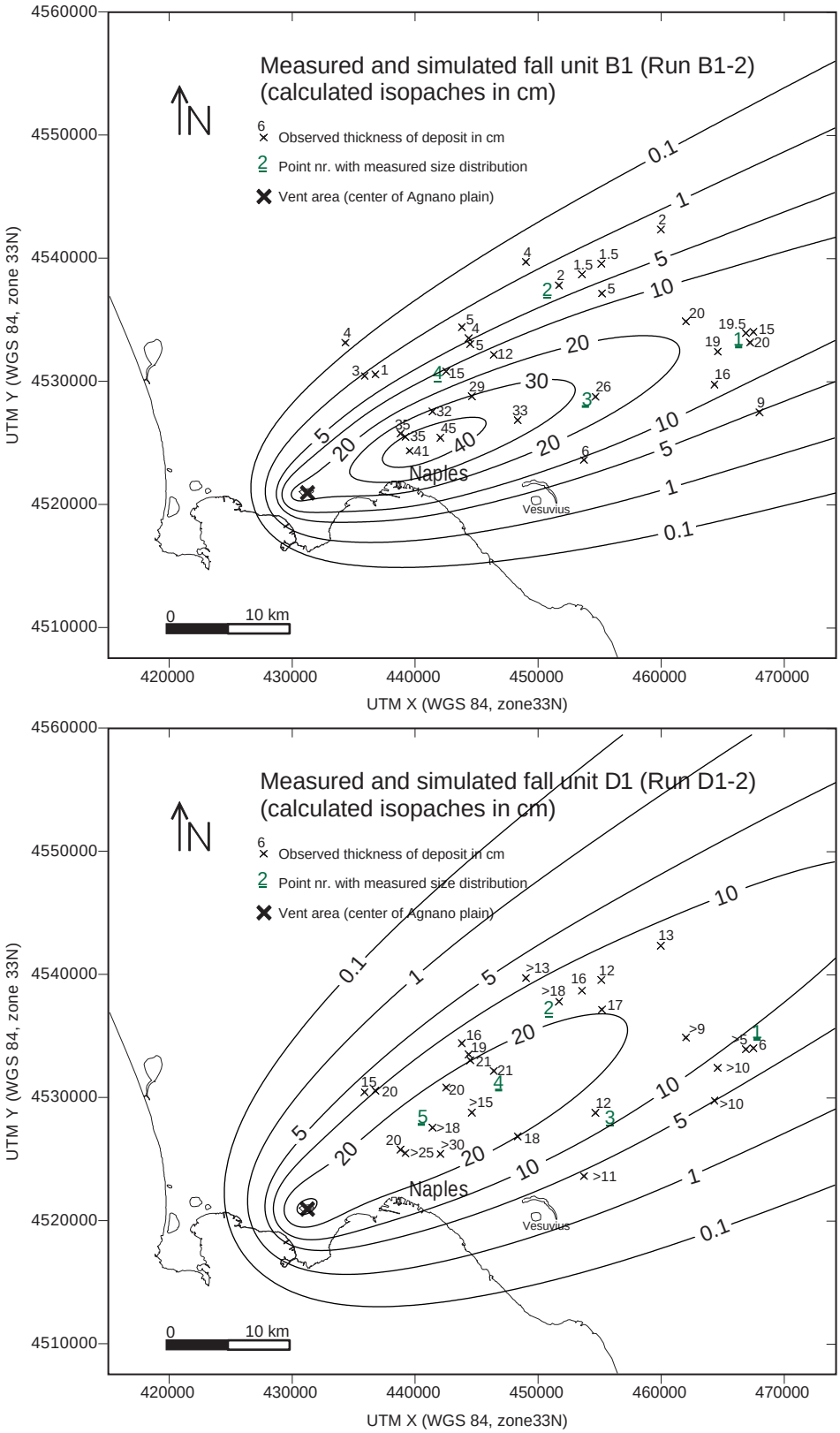

Fig. 5. Calculated isopachs and measured deposit thickness in cm of B1 and D1 fall deposit for Runs B1-2 and D1-2 (Wind model 2).

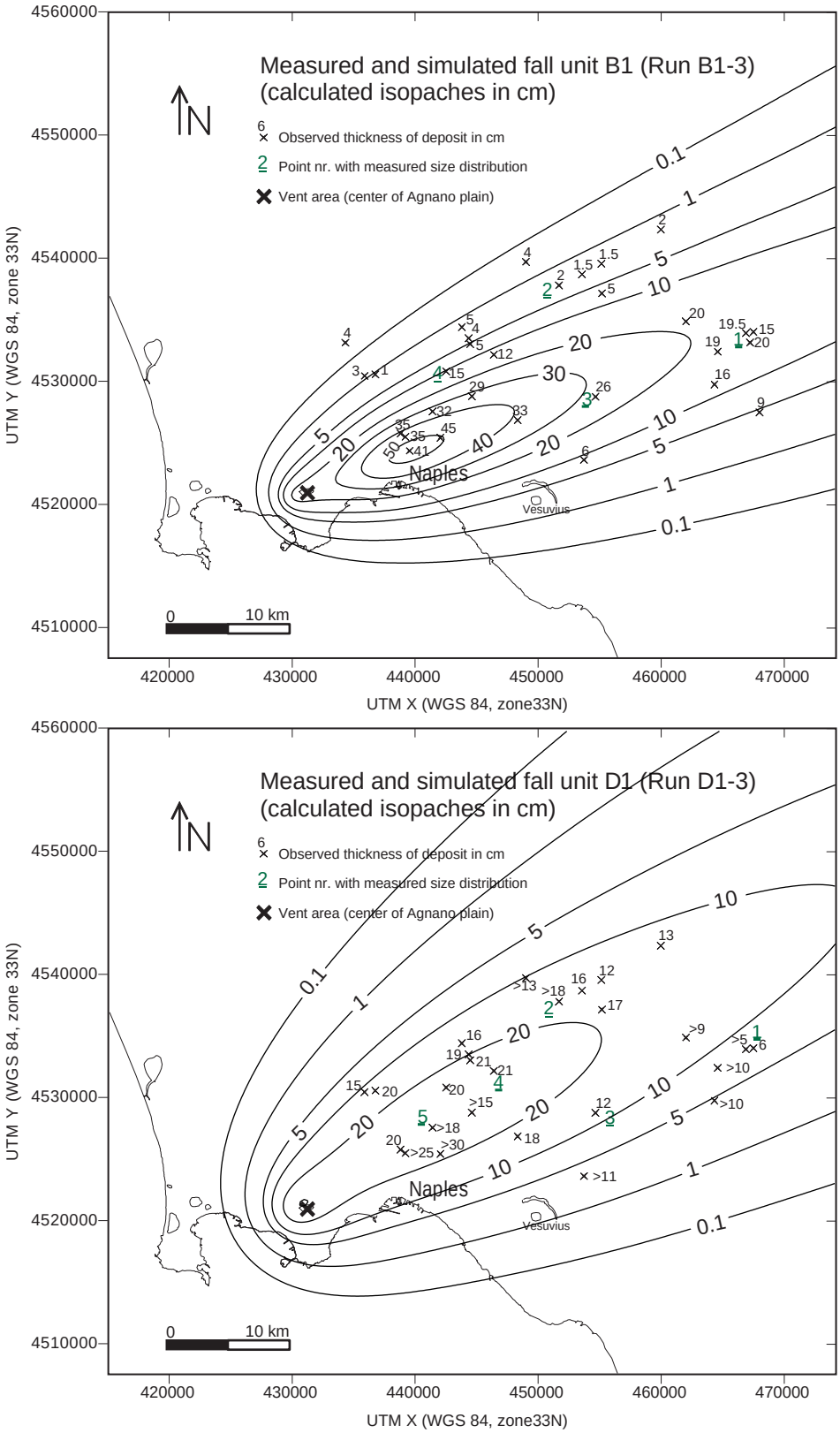

Fig. 6. Calculated isopachs and measured deposit thickness in cm of B1 and D1 fall deposits for Runs B1-3 and D1-3 (Wind model 3).

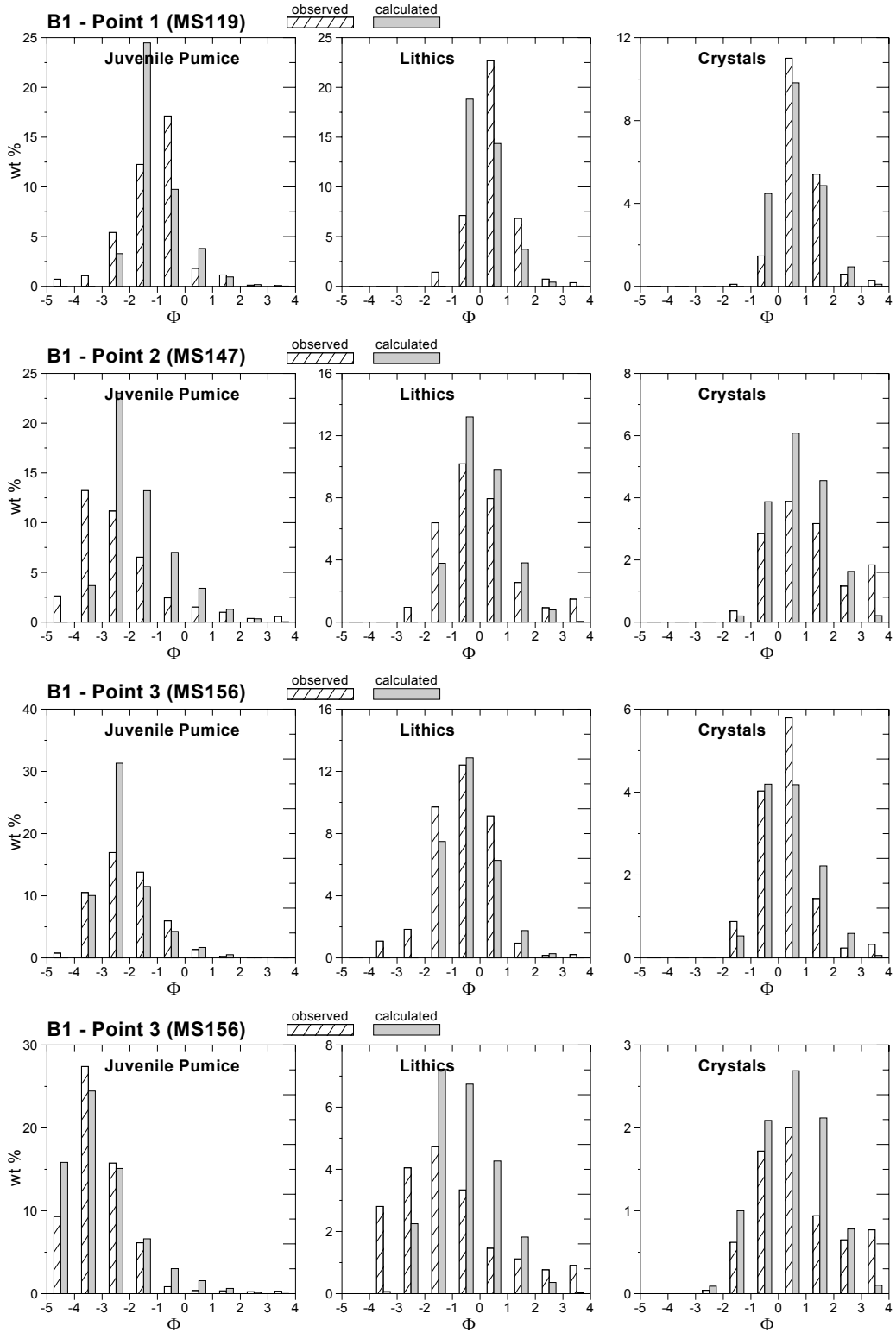

Fig. 7. Component and grain-size distribution for Run B1-1 (wind model 1).

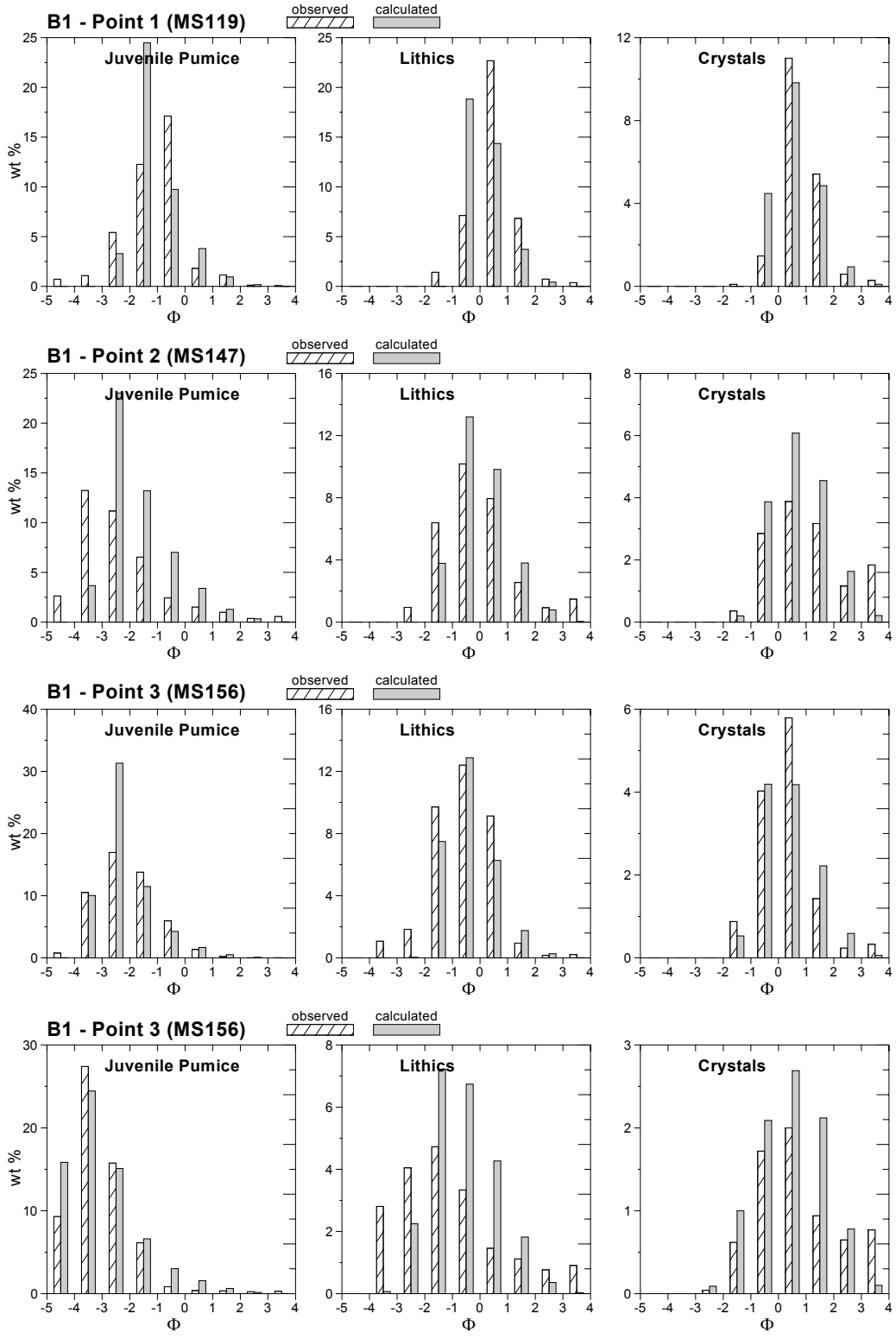

Fig. 8. Comparison with field data of the component and grain-size distribution for Run B1-1 (wind model 1).

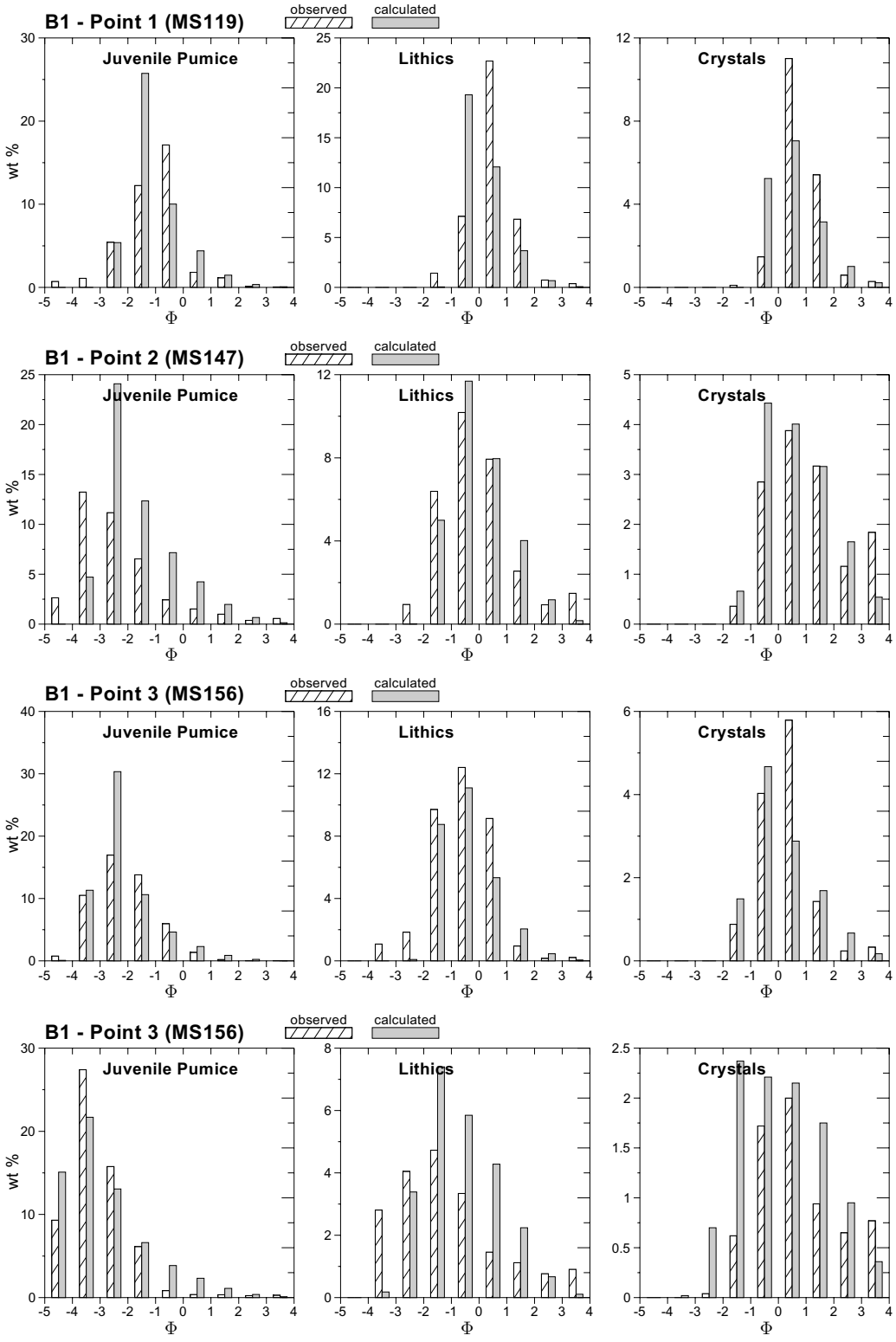

Fig. 9. Comparison with field data of the component and grain-size distribution for Run B1-2 (wind model 2).

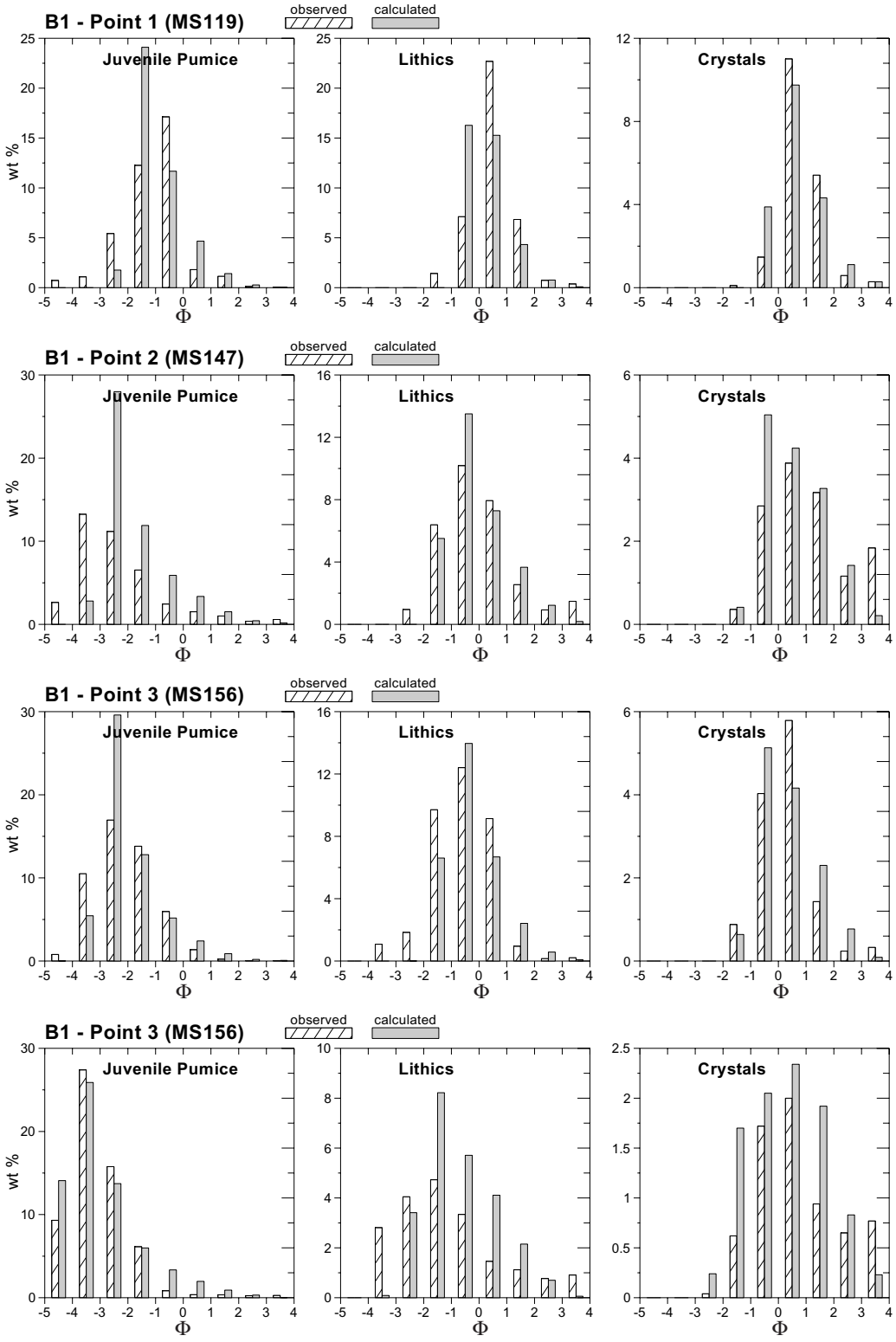

Fig. 10. Comparison with field data of the component and grain-size distribution for Run B1-3 (wind model 3).

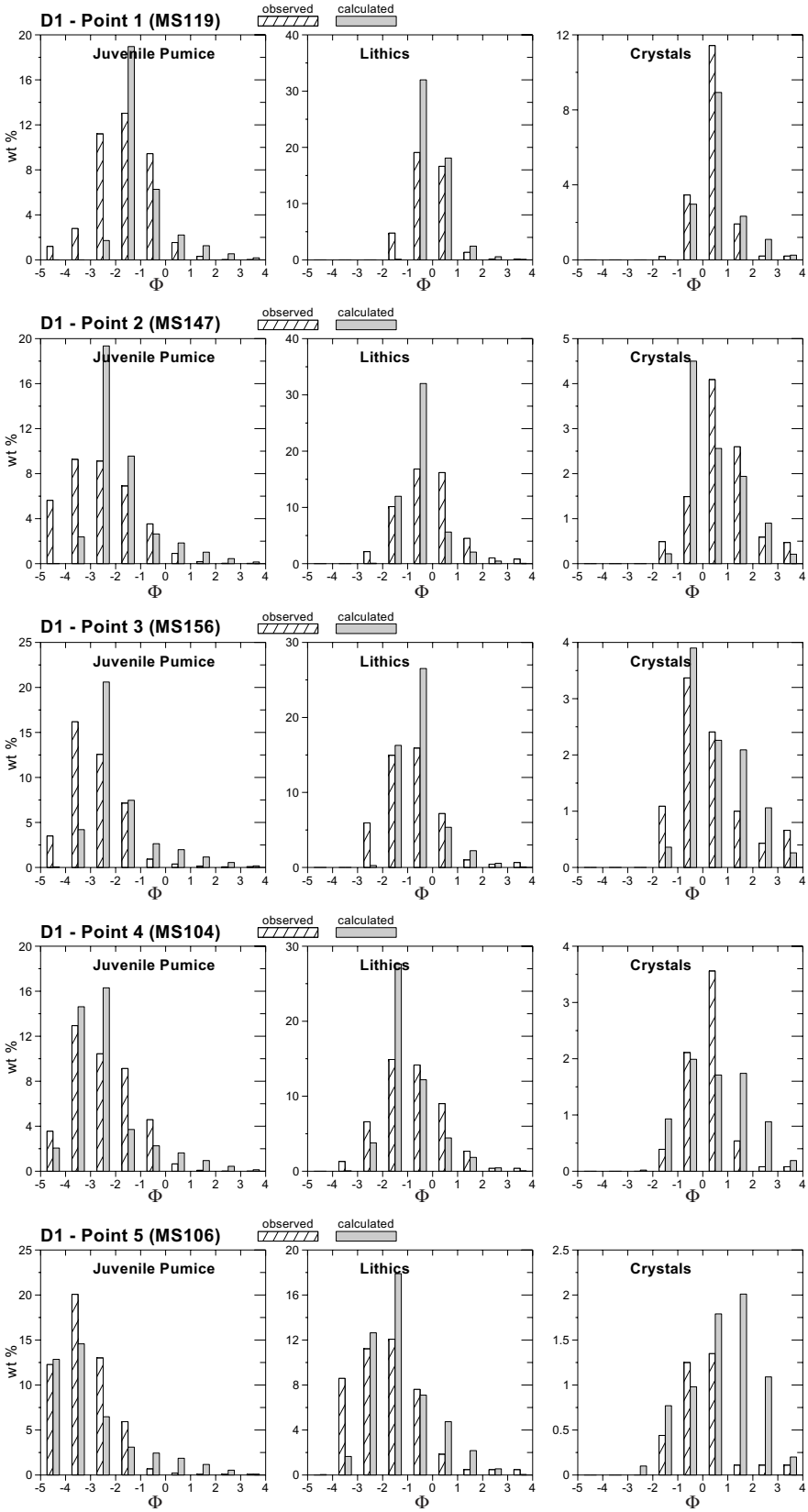

Fig. 11. Comparison with field data of the component and grain-size distribution for Run D1-1 (wind model 1).

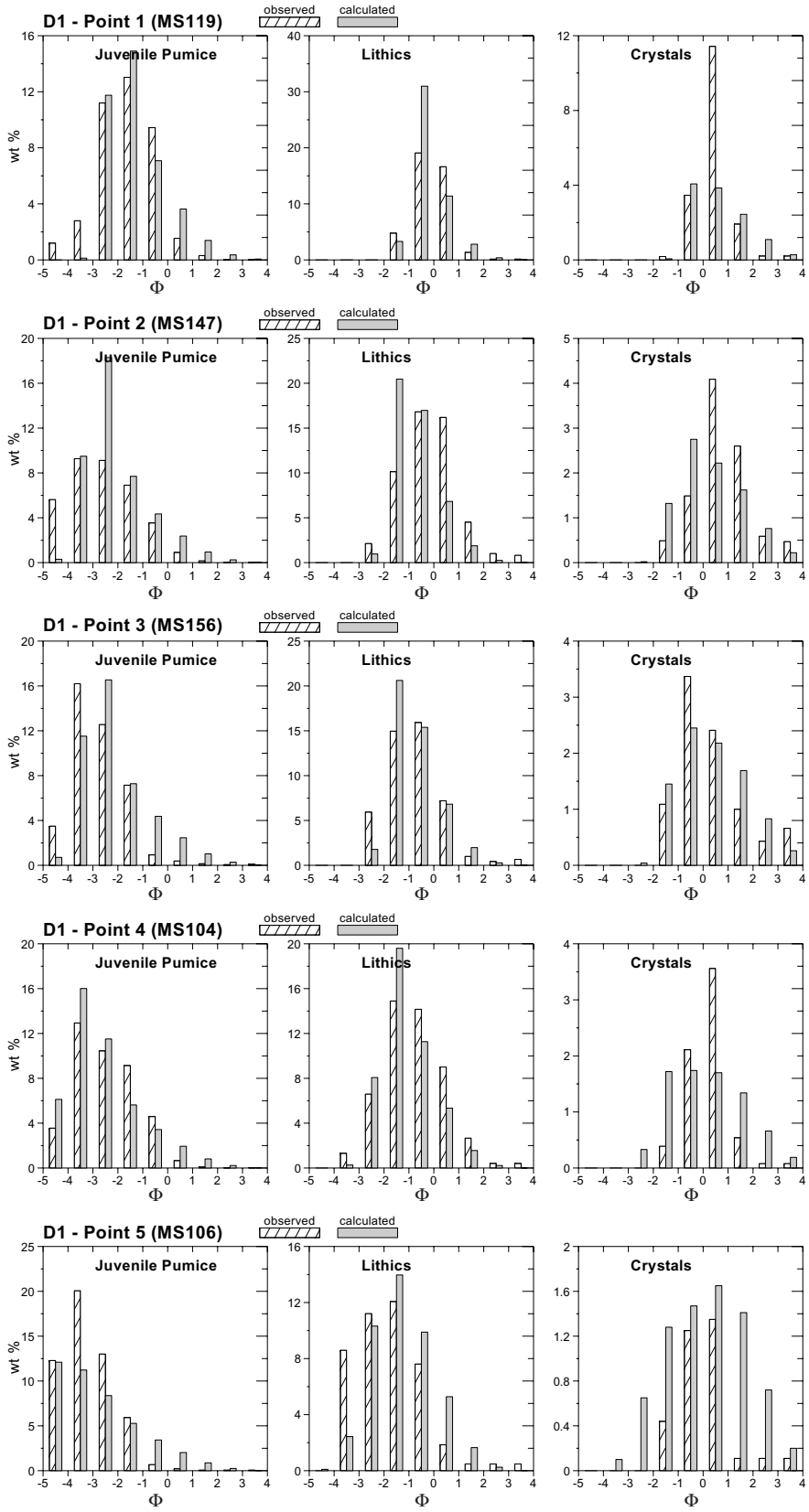

Fig. 12. Comparison with field data of the component and grain-size distribution for Run D1-2 (wind model 2).

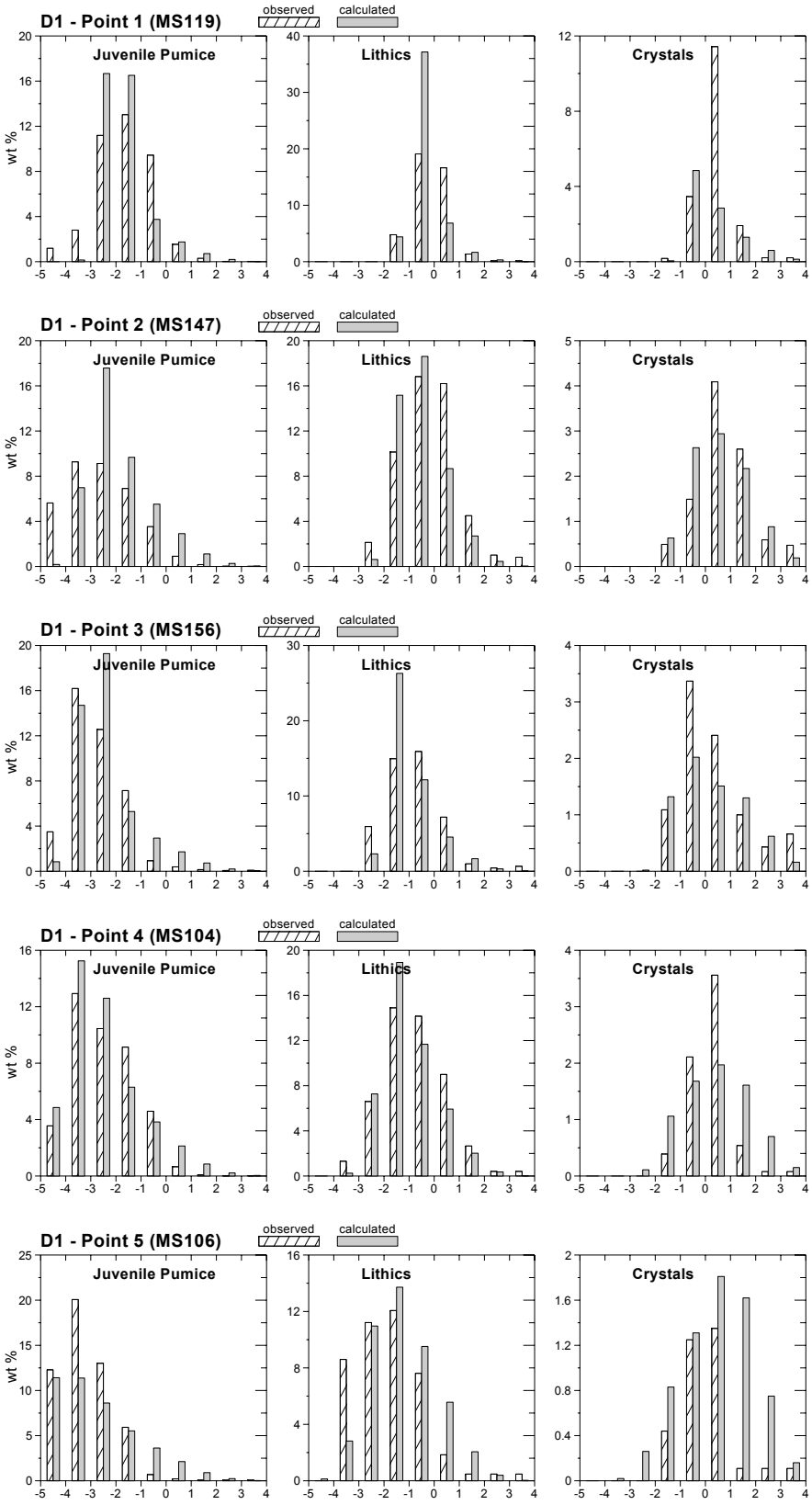

Fig. 13. Comparison with field data of the component and grain-size distribution for Run D1-3 (wind model 3).

Table 3: Comparison measured and calculated deposit B1 (Runs B1-1-3)

Pt. Nr.	Label in De Vita et al. (1999)	Measured thickness [cm]	Calculated deposit thickness (assuming 25% total vol. void fraction) [cm]			Calculated mass deposition [kg/m^2]	Calculated Density [g/cm3]	Measured Density
			B1-1	B1-2	B1-3		B1-1	
1	MS119	**15**	14.6	14.7	15.6	132	0.91	not measured
2	MS147	**2**	2.8	2.7	2.4	22	0.80	n. m.
3	MS156	**26**	24.9	25.2	25.5	176	0.71	0.74
4	MS122	**15**	10.3	9.9	9.7	66	0.65	0.65
5	MS106	**32**	30.2	29.0	31.7	180	0.60	n. m.
6	MS104	**12**	11.9	11.8	11.9	80	0.68	n. m.
7	MS107	**35**	36.2	34.0	38.9	206	0.57	n. m.
8	MS111	**29**	28.7	28.1	30.6	179	0.63	n. m.
9	MS114	**45**	43.5	41.6	47	254	0.58	n. m.
10	MS123	**33**	33.7	33.5	36	218	0.64	n. m.
11	MS127	**4**	0.1	0.0	0	0	0.98	n. m.
12	MS125	**3**	1.1	1.1	0.7	8	0.70	n. m.
13	MS136	**1**	1.6	1.5	1.1	11	0.69	n. m.
14	MS173	**35**	39.9	37.5	43.2	227	0.57	n. m.
15	MS172	**41**	44.8	42.1	49.2	254	0.57	n. m.
16	MS165	**4**	4.1	4.0	3.6	29	0.70	n. m.
17	MS164	**5**	5.5	5.3	4.9	38	0.69	n. m.
18	MS179	**5**	2.1	2.0	1.7	15	0.73	n. m.
19	Ms150	**6**	8.7	8.7	7.8	62	0.72	0.63
20	MS155	**4**	0.5	0.5	0.3	4	0.87	n. m.
21	MS174	**5**	6.5	6.5	6.4	52	0.79	n. m.
22	MS121	**16**	12.0	12.1	11.8	103	0.86	n. m.
23	MS117	**19**	15.8	15.9	16.4	136	0.86	n. m.
24	MS145	**20**	16.1	16.3	17.3	136	0.84	n. m.
25	MS149	**19. 5**	14.9	15.0	16	134	0.90	n. m.
26	MS115	**20**	14.2	14.3	15	128	0.90	n. m.
27	MS146	**9**	4.7	4.6	4.2	43	0.92	n. m.
28	New data	**1.5**	2.5	2.5	2.2	21	0.82	n. m.
29	New data	**1.5**	2.3	2.3	2	20	0.85	n. m.
30	New data	**2**	1.8	1.7	1.6	16	0.93	n. m.

Table 4: Comparison measured and calculated deposit D1 (Runs D1-1-3)

Pt. Nr.	Label in De Vita et al. (1999)	Measured thickness [cm]	Calculated deposit thickness (assuming 25% total vol. void fraction) [cm]			Calculated mass deposition [kg/m^2]	Calculated Density [g/cm3]	Measured Density
			D1-1	D1-2	D1-3		D1-1	
1	MS119	**6**	6.8	7.0	6.9	69	1.02	not measured
2	MS147	**>18**	15.8	15.7	15.5	144	0.91	0.78
3	MS156	**12**	11.6	12.7	11.5	104	0.90	0.77
4	MS104	**21**	23.6	23.9	23.2	201	0.85	n.m.
5	MS106	**>18**	26.4	27.1	25.4	214	0.81	n.m.
6	MS107	**20**	25.0	26.1	24.3	199	0.80	n.m.
7	MS111	**>15**	25.9	26.8	24.8	216	0.83	n.m.
8	MS114	**>30**	22.7	23.8	20.6	185	0.81	n.m.
9	MS122	**20**	23.0	22.4	22.9	192	0.83	0.79
10	MS125	**15**	9.3	8.2	10.6	78	0.84	n.m.
11	MS136	**20**	11.1	9.8	12.4	92	0.83	n.m.
12	MS173	**>25**	24.8	26.0	23.7	198	0.80	n.m.
13	MS150	**>11**	3.8	3.7	3.1	34	0.90	n.m.
14	MS155	**>13**	9.9	8.5	9.5	89	0.91	n.m.
15	MS174	**17**	17.3	18.5	17.3	162	0.94	n.m.
16	MS121	**>10**	4.3	4.4	4.4	44	1.01	n.m.
17	MS117	**>10**	7.0	7.4	7.2	70	1.01	n.m.
18	MS145	**>9**	12.0	13.3	12.4	119	0.99	n.m.
19	MS149	**>5**	7.1	7.4	7.3	72	1.02	n.m.
20	MS165	**19**	18.8	17.6	18.6	160	0.85	n.m.
21	MS164	**21**	20.2	19.3	20.0	172	0.85	n.m.
22	MS179	**16**	15.4	13.8	15.4	132	0.86	n.m.
23	new data	**16**	15.0	15.0	14.6	140	0.93	n.m.
24	new data	**12**	14.4	14.3	13.8	137	0.96	n.m.
25	new data	**13**	12.8	12.4	11.7	128	1.01	n.m.